J. Fluid Mech. (1985), *vol.* 159, *pp.* 69–84
Printed in Great Britain

Resonant and non-resonant waves excited by periodic vortices in airflow over water

By J. P. GIOVANANGELI AND A. MEMPONTEIL
Institut de Mécanique Statistique de la Turbulence, Laboratoire Associé au C.N.R.S. No. 130, 12, Avenue du Général Leclerc, 13003 Marseille, France

(Received 19 January 1984 and in revised form 15 March 1985)

This paper describes an experimental study, conducted in the I.M.S.T. air–sea interaction tunnel, of waves excited on a water surface by a periodic train of vortices in the air flow above. The water surface, under some conditions, shows a rapidly developing resonant response, while in the non-resonant case waves propagate both upstream and downstream at speeds different from, but dependent upon, the vortex-convection speed.

1. Introduction

The generation of waves by wind is now known to represent a mélange of physical processes, each of which contributes in some way or another to the development of the overall wave field. For example, the statistical mechanics of wave–wave interactions (Hasselmann 1968) is involved in energy transfer among different components; the influence of finite steepness on wave generation has been described by Longuet-Higgins (1977); and Mollo-Christensen & Ramamonjiarisoa (1978) explored the behaviour and nature of finite wave groups. The initial generation of waves on a sea that is initially calm seems still to be described by the resonance mechanism (Phillips 1957; Gelci, Ramamonjiarisoa & Hervouet 1983) augmented by Miles' (1960) feedback mechanism as the waves develop. However, the existence of the resonance mechanism has not been demonstrated explicitly because of the difficulty in providing a detailed description of the surface-stress fluctuations in a natural turbulent boundary layer.

The main purpose of this paper is to report on the results of an experimental study in which the surface-stress distribution is controlled experimentally. These results confirm the occurrence of the resonance phenomenon in wave generation. The paper also presents new results on the evolution of non-resonant waves.

2. Theoretical background

Lamb (see Stoker 1957) seems to be one of the first authors to study the response of a water surface subject to a moving pressure field propagating above it. The analysis is linear and shows that the wave amplitude is a maximum if the resonance condition is satisfied, i.e. if the propagation speed of the waves is equal to that of the pressure field. The Phillips (1957) analysis represents in some ways an extension of Stoker's model to the more realistic case of a turbulent wind blowing over the air–water surface. This analysis is also linear and is based essentially on a representation of the air-flow perturbations associated with the turbulent motions, the surface-

pressure field being directly connected to the vortex motions in the turbulent boundary layer which are convected above the surface. Phillips showed again that the resonance process seems to be the main mechanism which leads to the generation of the initial wind waves.

Recently Gelci *et al.* (1983) developed a numerical model to analyse the response of a water surface under the effect of a vortex street in the adjacent air flow. The description of the air-flow perturbations is similar to that proposed by Phillips in so far as it concerns a vortex distribution convected by a mean flow. However, the analysis avoids linearization of the equations, essentially by using vortex theory. The first results concerning waves of small slope agree rather well with those of Phillips' model.

The simple analysis below summarizes the main results for both resonant and non-resonant conditions. Let us suppose that when $t > 0$ a pressure wave

$$p = H \exp \mathrm{i}(\omega t - kx)$$

is applied to the surface, which is initially at rest. The propagation speed $W = \omega/k$. During the initial stages it can be supposed that the wave slope is sufficiently small to justify the linearization of the kinematical and dynamical boundary conditions so that the motion is governed by the following set of equations:

$$\left.\begin{gathered} \nabla^2\phi = 0; \\ \frac{\partial\eta}{\partial t} = \frac{\partial\phi}{\partial z}; \quad \frac{p}{\rho} = \frac{\tau}{\rho}\frac{\partial^2\eta}{\partial x^2} - g\eta - \frac{\partial\phi}{\partial t} \quad \text{at } z = 0; \\ \phi \to 0 \quad \text{as} \quad z \to -\infty; \end{gathered}\right\} \tag{1}$$

where ϕ is the velocity potential corresponding to the irrotational water flow, η the interface-level fluctuations, x and z respectively the horizontal and vertical coordinates, p the air-pressure fluctuations, ρ the water density, τ the surface tension at the interface and g the gravitational acceleration. The surface response is necessarily of the form $\eta = \eta(t)\, \mathrm{e}^{-\mathrm{i}kx}$, and, from a combination of the above equations, it is found that

$$\frac{\mathrm{d}^2\eta(t)}{\mathrm{d}t^2} + \alpha^2\eta(t) = A\, \mathrm{e}^{\mathrm{i}\omega t}, \tag{2}$$

where $A = -kH/\rho$, $\alpha^2 = (gk + \tau k^3/\rho)$, as given by Phillips. It represents a linear oscillator with natural frequency α subject to the external excitation $A\, \mathrm{e}^{\mathrm{i}\omega t}$.

First, consider the non-resonant case. If $\alpha \neq \omega$ the solution to (2), subject to initial conditions $\eta = \partial\eta/\partial t = 0$, is, taking the real part,

$$\eta = (\alpha - \omega)^{-1}\frac{kH}{2\rho\alpha}\cos(kx - \alpha t) + (\alpha + \omega)^{-1}\frac{kH}{2\rho\alpha}\cos(kx + \alpha t) - (\alpha^2 - \omega^2)^{-1}\frac{kH}{\rho}\cos(kx - \omega t), \tag{3}$$

representing freely travelling waves moving in both directions with speed $C = \alpha/k$ and the forced, non-resonant wave moving at the speed $W = \omega/k$ of the pressure distribution. In the case of resonance, with $\alpha = \omega$, the solutions under the same initial conditions can be represented as

$$\eta = -\frac{kH}{2\rho\omega^2}\cos kx \cos\omega t - \frac{kH}{4\rho\omega}t \sin(\omega t - kx), \tag{4}$$

in which the first term represents a standing wave, or the superposition of two identical waves moving in opposite directions, and the second term is the resonant wave moving downstream with speed $W = C$, its amplitude growing linearly with time. The same components appear in Gelci *et al.*'s (1983) study.

Equation (3), corresponding to non-resonant case, can be written as:

$$\eta_R \simeq \frac{kH}{2\rho(\omega^2-\alpha^2)}\left\{\sin\left(\frac{\omega-\alpha}{2}\right)t\right\}\left\{\sin\left(kx-\left(\frac{\alpha+\omega}{2}\right)t\right)\right\} + \frac{kH}{2\rho(\omega^2-\alpha^2)}\left\{\sin\left(\frac{\omega+\alpha}{2}\right)t\right\}\left\{\sin\left(kx+\left(\frac{\alpha-\omega}{2}\right)t\right)\right\}. \quad (5)$$

The first term of the right-hand side of (5) represents a wave propagating downstream with the phase celerity $\frac{1}{2}(C+W)$. The wave amplitude is modulated in time at the period $\theta_m = 2L/(C-W)$. The second term represents a wave propagating downstream or upstream at the celerity $\frac{1}{2}(W-C)$ with amplitude modulated in time at the period $\theta'_m = 2L/(C+W)$, with $L = 2\pi/k$.

In this simple analysis the amplitude of the pressure wave is equal to 0 for $t < 0$ and H for $t > 0$. In nature H can depend gradually on time, for example in a gust or in the initial movement of the wind. If the magnitude of the pressure wave increases from zero to a constant value during a time T, it can be shown that in the non-resonant case the amplitude of the free wave is proportional to T^{-1}; for large values of T this amplitude is small. Consequently, in nature, a non-resonant pressure pulsation coming and going would generate forced waves, but hardly free waves.

An experiment has been conducted in a wind–water tunnel to test these results. It has been possible to study the behaviour of an air–water interface submitted to the direct interaction of a distribution of vortices in the air flow above the surface which moved over it at different velocities.

3. Experimental arrangement

3.1. *The wind–wave tank and the experimental conditions*

The experiments were conducted in the $\frac{1}{5}$-scale model of the large I.M.S.T. wind–wave tank described in detail by Favre & Coantic (1974).

A key part of the investigation was the development of a device capable of generating perturbations with controllable dynamical and kinematical properties in the air flow. Within the context of the analysis presented above the air-flow perturbations were designed to be a row of vortices which satisfied, as far as possible, the following criteria: (*a*) the vortex strength had to be sufficient to generate a significant interfacial motion; (*b*) the vortex field had to be sufficiently stable to survive downstream of the vortex generator without significant change of its main characteristics; and (*c*) the convection velocity of the vortices had to include values satisfying the resonance condition.

A review of earlier theoretical and experimental work (Goldstein 1957; Betchov & Criminale 1967; Wood & Kirmani 1970) suggested that naturally occurring vortices in a boundary layer do not simultaneously satisfy these criteria. Consequently, a technique which allows the vortex-generation frequency to be independent of the wind velocity is necessary. A series of preliminary tests was carried out to find, first, an approximate vortex-generating device and then to discover suitable experimental conditions. The final experimental configuration is shown on figure 1.

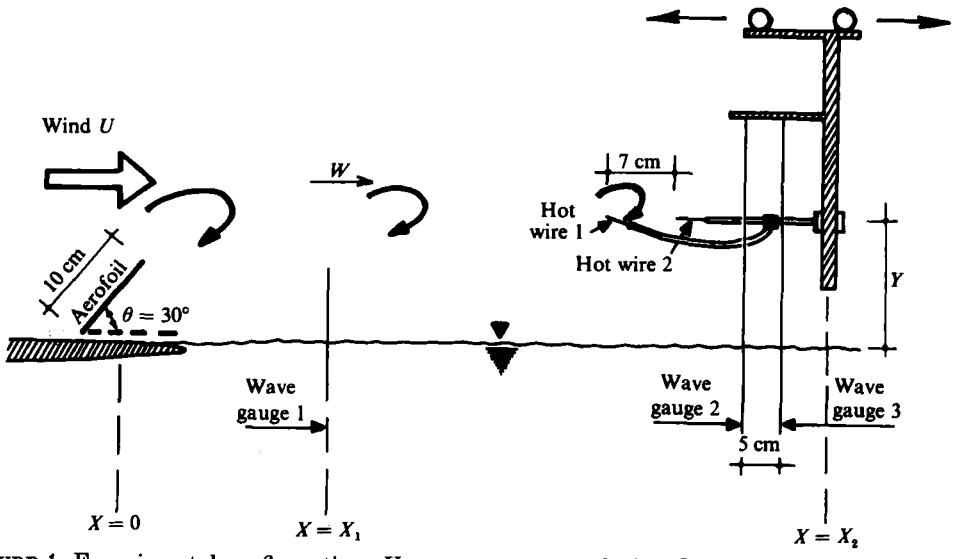

FIGURE 1. Experimental configuration: U mean upstream velocity, W convection velocity of the vortex distribution, X fetch, Y distance of the hot wires above the surface.

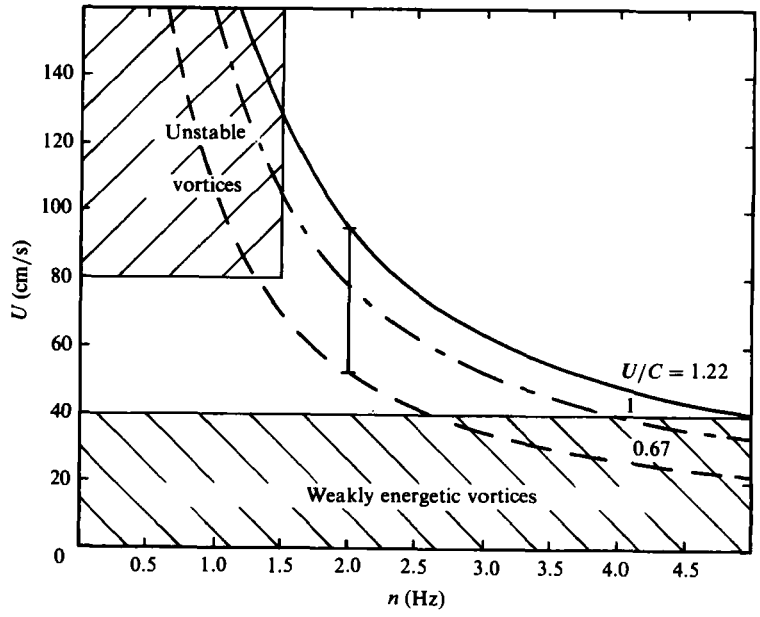

FIGURE 2. Experimental conditions: ▨, domain of unstable vortices; ▨, domain of weakly energetic vortices; n is the oscillation frequency of the aerofoil.

The vortex generator used was a two-dimensional flapping aerofoil of 10 cm chord placed above the upstream beach of the wind–wave tank. In this way, the perturbations in the immediate vicinity of the aerofoil do not perturb the water surface. The aerofoil oscillated between a horizontal position and a maximum angular displacement θ. A sensor measured the instantaneous value of the displacement.

With this vortex generator we made an extensive search to find a range of the vortex-generator frequency n and wind velocity U to satisfy, as far as possible, the

requirements listed above. Figure 2 shows the results of this investigation. In the range $U > 0.80$ m/s, $n < 1.50$ Hz approximately, the vortices were found to be highly unstable and their main characteristics (convection velocity, associated velocity fields, etc.) evolved quite rapidly downstream. In the range $U < 0.40$ m/s, for all values of n, the vortices were found to be insufficiently energetic to produce significant water-surface motions. As shown on the figure, a small domain of n and U values exists where it appears possible to satisfy the various criteria. It was decided to run the experiment with $n = 2$ Hz and at a wind velocity ranging from 0.50 to 2 m/s approximately. The resonance condition could then be satisfied at U of order 0.80 m/s. The maximum angular displacement θ was of order 30°. Under such conditions it was clearly seen, using a tobacco-smoke-visualization technique, that the aerofoil indeed produces a vortex at its trailing edge when it reached its highest position.

3.2. *The measuring devices*

The air-velocity fluctuations owing to the vortex motion were measured using two single hot wires with DISA model 55 constant-temperature anemometers. As shown on figure 1 the wires were 7 cm apart horizontally. A special probe support was used to minimize the effect of the wake of the upstream probe on the downstream probe. The experimental conditions were such that the air-velocity field had small mean values but large amplitude fluctuations. The use of digital techniques for data acquisition and processing were necessary. The hot wires were calibrated for velocities ranging from 0.01 to 5 m/s. At very low velocities an air tank was used equipped with a rotor on which was mounted the hot wire; while at higher velocity the calibration was made in a small wind tunnel with controllable temperature and velocity. A least-square-regression calculation, as proposed by Giovanangeli (1980), was used to find the Collis & Williams (1959) cooling law of the hot wires.

The water-surface deflection was measured using capacitance wave gauges of 0.3 mm outer diameter with DISA model 55E capacitance measuring units. The gauges were mounted on a movable carriage to record the variations at any desired fetch value (figure 1). The typical sensitivity of the probes was of order 0.6 volt/cm. This high sensitivity was necessary for accurate measurements of the small amplitudes of the vortex-induced waves. The wave gauges were calibrated repeatedly during the experiments by raising and lowering them by known amounts.

4. Data processing

The output voltages of the sensors were stored numerically on a Hewlett-Packard model 2100A computer after digitization at 40 Hz sampling frequency. Low-pass analog linear filters were used prior to digitization to prevent aliasing. Fast-Fourier-transform techniques were used to estimate statistical properties such as spectra and cross-spectra. An estimate of the phase celerity $C(n)$ was made on the basis of the classical formula

$$C(n) = \frac{2\pi \Delta x\, n}{\Phi(n)}, \tag{6}$$

where n is the frequency, Δx the distance between two probes and $\Phi(n)$ the phase of the cross-spectral density of the signal from the two probes.

Most of our observations were carried out at constant wind velocity and the data were analysed using standard fast-Fourier-transform methods (FFT) applicable to stationary processes. We also did a series of experiments under non-stationary

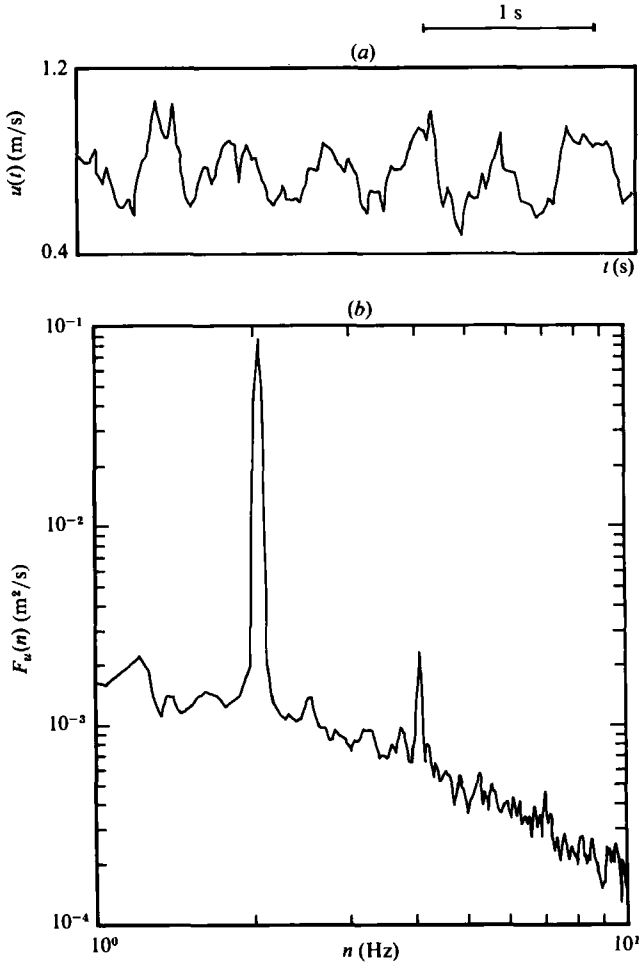

FIGURE 3. (*a*) Time variation of the longitudinal component u of the air velocity for $U = 0.83$ m/s and (*b*) the corresponding power-spectral density.

conditions, under rapidly increasing wind speed. The data from these experiments were analysed using maximum-entropy methods.

The basic concept of the procedure has been presented by various authors (Burg 1968; Ulrych & Jensen 1974; van den Bos 1971; Lacoss 1977) and does not need to be recalled here. The procedure is known to be especially valuable for peak resolution and for spectral estimation using samples of short duration.

We also extended the use of the maximal-entropy concept to estimation of the cross-spectral-density function of two random variables of small time duration. This may be a new application of the concept. The essence of the method (Memponteil 1983) is the estimation of a transfer function between the two variables, compatible with the concept. Then a phase was defined and a phase celerity computed by a formula such as (6). Finally, 'instantaneous' variances, spectral- and cross-spectral-density functions were obtained by using samples of order 3.2 s duration.

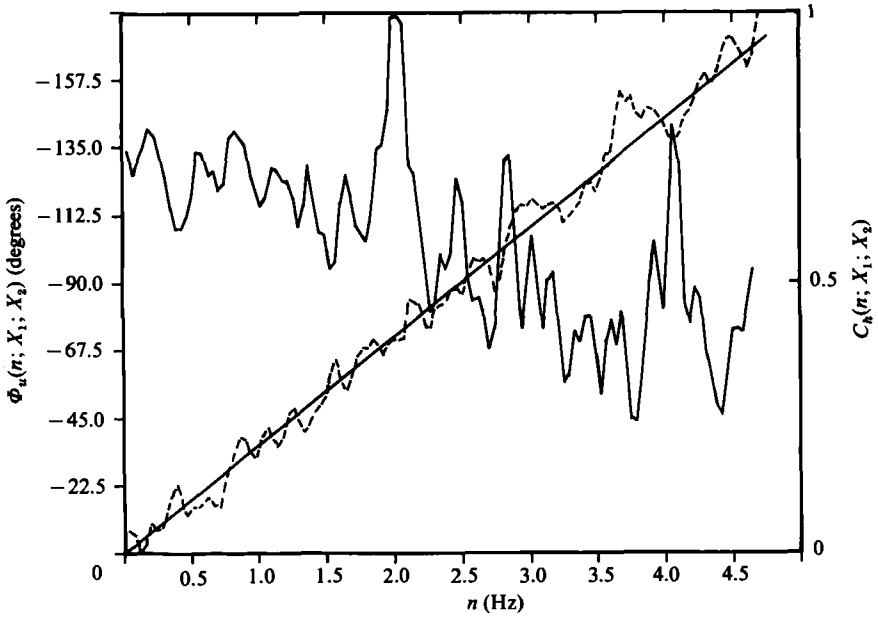

FIGURE 4. Cross-spectral density of the air-velocity fluctuation at $X_1 = 0.57$ m and $X_2 = 0.64$ m: ---, phase $\Phi_u(n; X_1; X_2)$; ——, coherence $C_h(n; X_1; X_2)$.

5. Experimental results

5.1. *The air-flow-perturbation field*

The observations were made first at fetch $X_1 = 0.57$ m and later at fetch $X_2 = 1.565$ m, and for two different hot-wire heights above the water surface.

Figure 3 shows typical samples of the time dependence of the longitudinal component u of the air velocity at fetch X_1 for a mean velocity of 0.83 m/s, and the corresponding power-spectral-density function. There is clear evidence of the presence of quasi-periodic variations at the period of oscillation of the vortex generator. The spectrum exhibits two main peaks, one at the vortex-generator frequency and the other at the frequency of its second harmonic. The velocity oscillations are thus not sinusoidal.

The cross-spectral-density function of the air-velocity fluctuations at the two fetches X_1 and $X_1 + \Delta X_1$ ($\Delta X_1 = 7$ cm) is shown on figure 4. The coherence function, like the power-spectral density, has two main peaks, at 2 Hz and 4 Hz respectively. The coherence value is almost unity at 2 Hz. The phase shift in u between X_1 and $X_1 + \Delta X_1$ is approximately proportional to the frequency.

At first sight this suggests that the perturbations in the air flow advance downstream as a disturbance of permanent form. However a detailed inspection of the waveform and the spectral density shown on figure 3, as well as the coherence function shown on figure 4, make it difficult to relate a simple physical mechanism to the oscillations at frequencies below 2 Hz or between 2 and 4 Hz or above 4 Hz. For that reason it was found preferable to estimate the convection velocity W to be associated with the perturbation by the phase celerity, as defined by (5), at 2 Hz, the frequency at which the coherence function is a maximum. Because of the linear variation of the phase cited previously, the same celerity value would be found for

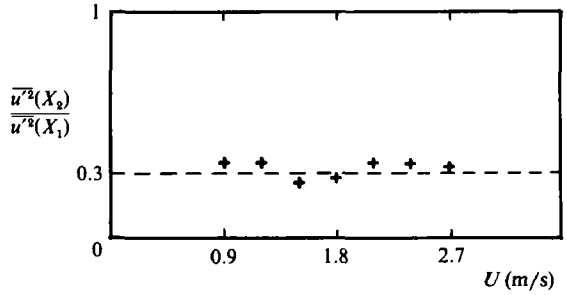

FIGURE 5. Vortex breakdown between $X = X_1$ and $X = X_2$ for different values of U; $X_1 = 0.50$ m, $X_2 = 1.25$ m.

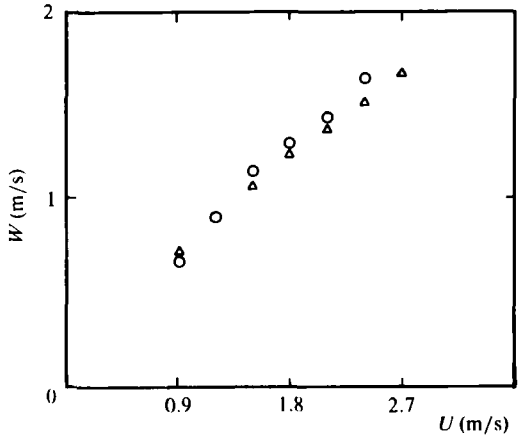

FIGURE 6. Vortex-convection velocity for different values of U: △, $X = 0.50$ m; ○, 1.25 m.

all other frequencies and, in particular at 4 Hz, the frequency of the second harmonic perturbation.

As far as the lifetime of the perturbation is concerned it was found (figure 5) that the variance $\overline{u'^2}$ of the velocity fluctuations decreases by a factor of 0.3 between the fetch X_1 and the fetch X_2. As shown on figure 5 this damping ratio does not depend upon the mean-wind-velocity value. Except for this decrease in the perturbation energy, most of the results above were found to be still valid at fetch X_2.

Then a systematic investigation of the air-flow structure was made for a mean wind velocity ranging from 0.6 to 1.7 m/s. The principal result was that the variation of the longitudinal velocity component is in close agreement with the expected variation due to a passing vortex (see e.g. Sedov 1973). Furthermore, as shown on figure 6, the convection velocity W is proportional to the mean velocity U.

5.2. *Water-surface response*

Figure 7 shows, for $U = 0.83$ m/s, a typical example of the time dependence of the water deflection level η and the corresponding spectral-density function. The deflection is like $u'(t)$, quasi-periodic at the frequency of the vortex generator. The spectrum shows two main peaks, at the frequency of the vortex generator and at its second harmonic. These results hold for all values of the mean wind velocity in the range of interest. This means that the air-flow perturbation forces water waves at the frequency of disturbances in the air flow.

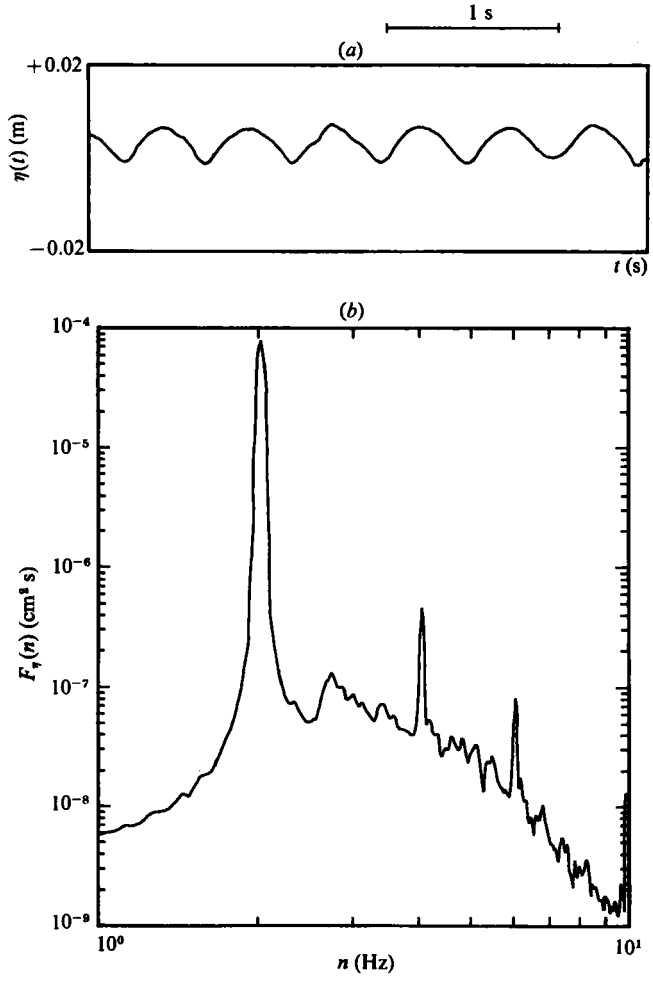

FIGURE 7. (*a*) Time variation of the water deflection level $\eta(t)$ for $U = 0.83$ m/s and (*b*) the corresponding power-spectral density function.

To describe the nature of the wave motion further (free or forced waves) the wave-phase celerity was measured at fetch X_2. This was done by calculating the cross-spectral density (see (5)). Figure 8 shows the results. It is seen that for a wind velocity in the range 0.8 to about 1.1 m/s the measured phase celerity C_m fits quite well with C_{th}, the value predicted by the linear theory. For the particular value $U = 0.86$ m/s of the wind velocity $C_m = W = C_{th}$. The wave would then be a resonant ($C_m = W$) free ($C_m = C_{th}$) wave. Otherwise, within the previous velocity range, the water-surface response consists of non-resonant ($C_m \neq W$), free ($C_m = C_{th}$) waves. For wind velocity higher than 1.1 m/s it is seen that the measured wave-phase celerity increases when the wind velocity increases. The departure from the theoretical value C_{th} becomes larger with increasing wind velocity. A detailed analysis of the observed evolution of the measured phase celerity is needed to specify the exact nature of the surface waves. A discussion follows.

As far as the dynamical properties of the observed vortex-induced waves are concerned, figure 9 displays the variance $\overline{\eta^2}(X_1)$, $\overline{\eta^2}(X_2)$ of the water-surface-deflection level as function of wave 'age' C/W, the amplification factor A defined as

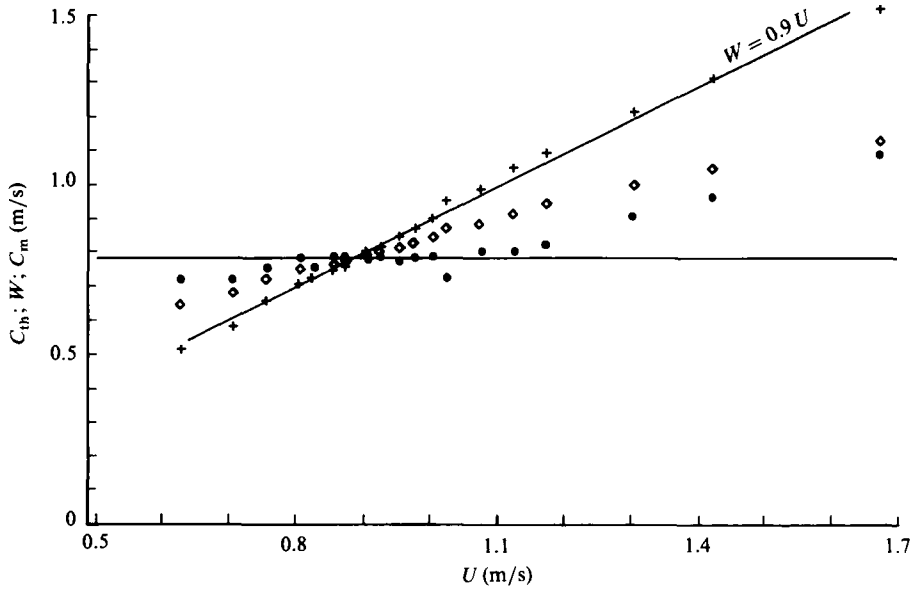

FIGURE 8. Wave-phase celerity and vortex-convection speed for different values of U: ——, theoretical wave-phase celerity C_{th}; —+—, measured vortex-convection velocity W; ●, measured wave-phase celerity C_m; ◇, $\frac{1}{2}(W+C_{th})$.

$(\overline{\eta^2}(X_2)-\overline{\eta^2}(X_1))/\overline{\eta^2}(X_1)$ is also shown. It is seen that the evolution of A has a large peak for C/W approximately equal to unity. Examining the evolution of the variance $\overline{\eta^2}(X_1)$ and $\overline{\eta^2}(X_2)$, the maximum in A corresponds to a maximum in wave amplification. Then these results confirm the existence of a resonance mechanism on the wave generation.

The highly selective character of the resonance mechanism is illustrated by the results shown on figure 10. The figure displays the evolution of the wave field with fetch for $C/W = 1.0$ and 0.9. For a meaningful comparison of the energy evolution for the two cases, the wave energy is divided by the air-flow kinetic energy. For fetches less than about 100 cm in both cases the wave energy first maintains an almost constant value and then increases rapidly. But for fetch higher than 100 cm there exists a large difference in the respective energy evolution: for $C/W = 1.0$ the energy still increases and then stabilizes at an almost constant value while for $C/W = 0.9$ the energy decreases rapidly.

Clearly the first case above corresponds, in principle, to a resonant condition for which the energy would increase linearly with fetch. The observed evolution has indeed a linear portion, but a stabilization seems to occur. A possible explanation for such unexpected behaviour is that, as shown previously, the vortices in the air have lost a large part of their energy and then became unable to maintain the wave amplification.

The second case corresponds to a non-resonant condition and a modulation in the wave amplitude is expected. It is quite remarkable that the experiments seem to confirm the existence of such modulation. The most striking observed fact is that a difference of order 0.1 in the wave-age value introduces a very significant change in the wave-energy evolution. The other fact is that, at least qualitatively, there is agreement between the analytical models and the observation.

From the quantitative viewpoint, for the non-resonant case, a simple calculation

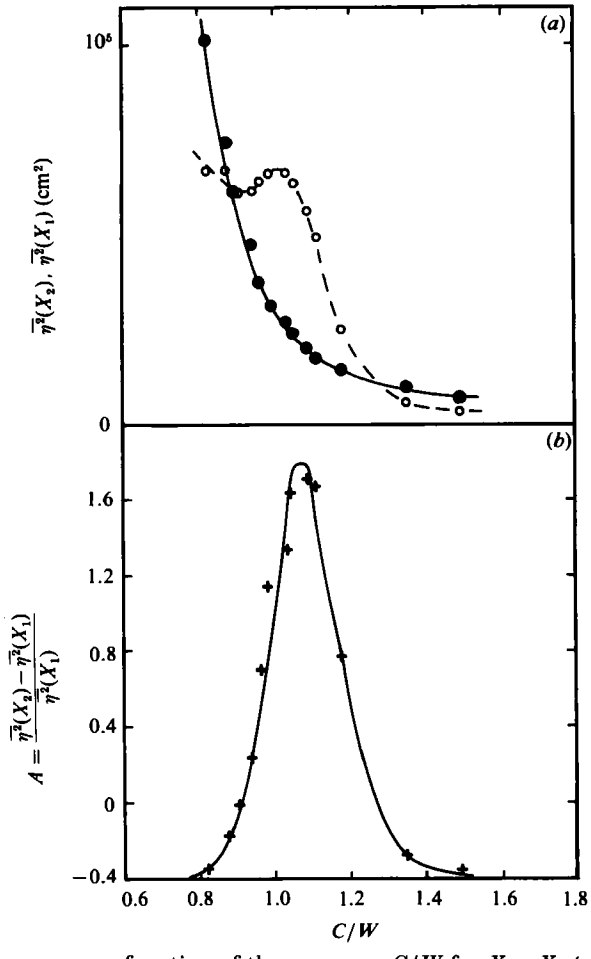

FIGURE 9. (*a*) Wave energy as function of the wave age C/W for $X = X_1$ (—●—) and $X = X_2$ (—○—). (*b*) Amplification factor A with respect to the wave age C/W.

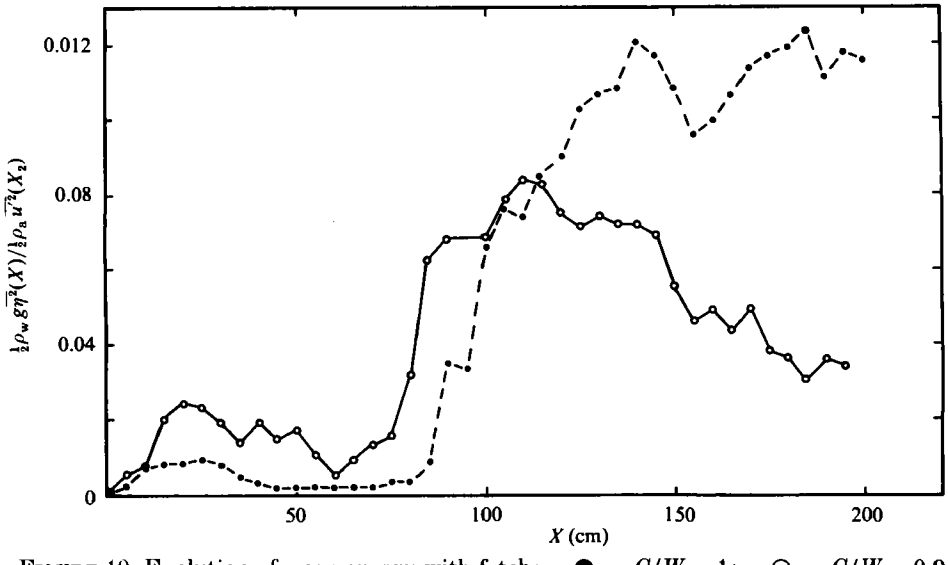

FIGURE 10. Evolution of wave energy with fetch: —●—, $C/W = 1$; —○—, $C/W = 0.9$.

allows one to show from the analytical models that the wavelength of the spatial modulation in wave energy is

$$X = \frac{LC_g}{|W-C|},$$

C_g being the group velocity of the non-resonant ($W \neq C$) free waves ($C = C_{th}$).

With the actual values ($C/W = 0.9$; $W = 0.865$ m/s; $C = 0.776$ m/s; $L = 0.43$ m), one finds $X = 1.87$ m. From figure 10, considering that the wave energy starts to increase at about $X = 0.6$ m, it is seen that such a value of the modulation wavelength is compatible with the observations.

6. Discussions and conclusions

The observations clearly showed the efficiency of the resonance mechanism for water-surface-wave generation under the action of the air-vortex motion, but there was also evidence of the formation of non-resonant waves, which may play a non-negligible role in the development of wind waves, a case of interest from the theoretical and practical viewpoint.

The efficiency of the resonance mechanism was checked for the more realistic case of a non-stationary wind flow. The experimental arrangement was identical with that shown on figure 1, except that the wind velocity was increased from 0 to about 3 m/s within 30 s. All the statistical properties of the wind and the wave fields were determined using spectral and cospectral analysis based on the maximum-entropy criterion (see e.g. Memponteil 1983). This made it possible to estimate the variance, the spectrum and the cospectrum of the physical variables using samples of about 3.2 s duration during the time-dependent evolution of the wave field.

Figure 11 shows the result for the wave amplification. The result is very similar to that for the stationary case, namely the wave amplification is a maximum at the resonance condition. This result is of interest for two reasons: first, the mechanism is still efficient for a non-stationary wind; and, secondly, the water surface responds almost instantaneously to the resonant excitation.

In the past many investigators focused their attention mostly on the resonant wave. However there is now some reason to believe that under certain circumstances the non-resonant wave may be of interest as well. As an example one may cite the case of the laboratory wind-generated waves which, in principle, cannot be considered as resonant waves, the wind velocity being generally much higher than the wave celerity. The dominant component of such wave fields would be classified as non-resonant, free waves. But it is difficult to define precisely the other wave components.

During the present work it was found that, in the non-resonant case, the vortex-induced wave is neither a free wave nor a forced wave. The results in figure 8 suggest that the water-surface oscillation is a mixture of Fourier components. Both analytical models suggest that three main components (a downstream free wave, an upstream free wave and a downstream forced wave) would be present. Obviously classical spectral-data analysis is unable to separate the components. Rather the analysis will mix the components to give an 'overall' wave celerity which is to a large extent meaningless.

In order better to specify the exact nature of the water waves a simple procedure was used: the water-deflection level was recorded at many fetches starting from $X = 1.08$ m, successively separated downstream by a distance of 2 cm.

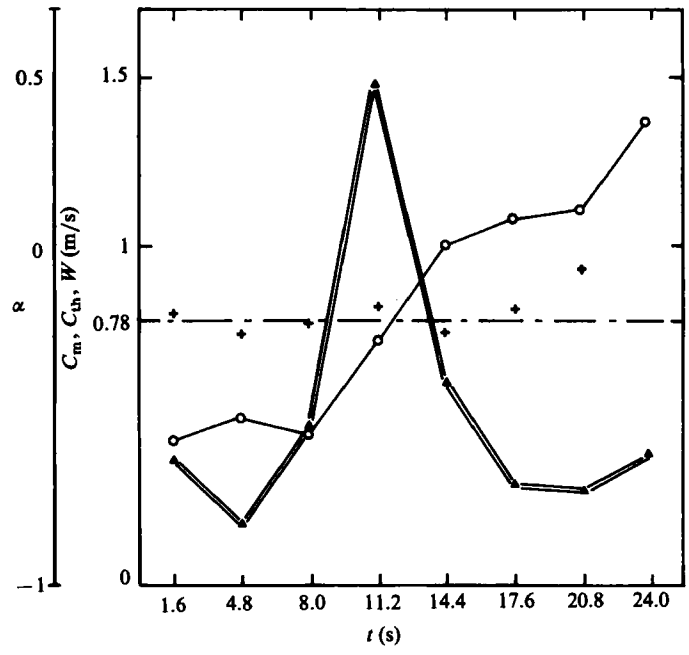

FIGURE 11. Amplification ratio α, theoretical and measured wave-phase celerity and vortex-convection velocity *versus* time for non-stationary conditions: =▲=, $\alpha = (\overline{\eta^2}(X_2) - \overline{\eta^2}(X_1))/\overline{\eta^2}(X_1)$; —O—, W; — — —, theoretical wave-phase celerity; +, measured wave-phase celerity.

Figure 12 shows the typical recorded waveforms with $W = 1.25$ m/s and $C/W = 0.73$. It is seen that, at a given fetch, a typical waveform consists of an oscillation with a large amplitude and much smaller bumps, indicated by the arrows; these are phase locked to the large oscillation. But the relative phase varies with fetch. In other words the interfacial deflection seems to contain two components propagating at different phase celerities. The phase celerity C_D of the large-amplitude component was determined by an elementary method consisting of measuring the phase shift between wave traces recorded simultaneously at two different fetches separated by a known downstream distance. A value $C_D = 1.04$ m/s was found.

The same procedure was found to be insufficiently accurate for determining the celerity C_R of the other component, the amplitude being too small and subject to a modulation, as expected from the analytical results. The following method was used:

Let k_R and k_D be, respectively, the wavenumbers corresponding to the small and the large oscillations and let Δx be the distance required for the combined oscillation to go through a complete cycle in its phase evolution. Then, one has

$$2\pi = |(k_R - k_D)|\,\Delta x$$

and

$$C_R = \frac{C_D\, n\, \Delta x}{C_D + n\, \Delta x},$$

n being the frequency of the oscillation under consideration, determined by the recorded time evolution of the wave profile and of order 2 Hz, the vortex-generator oscillation frequency.

From the traces shown on figure 12, Δx was estimated to be approximately 0.24 m. Then C_R is close to 0.32 m/s.

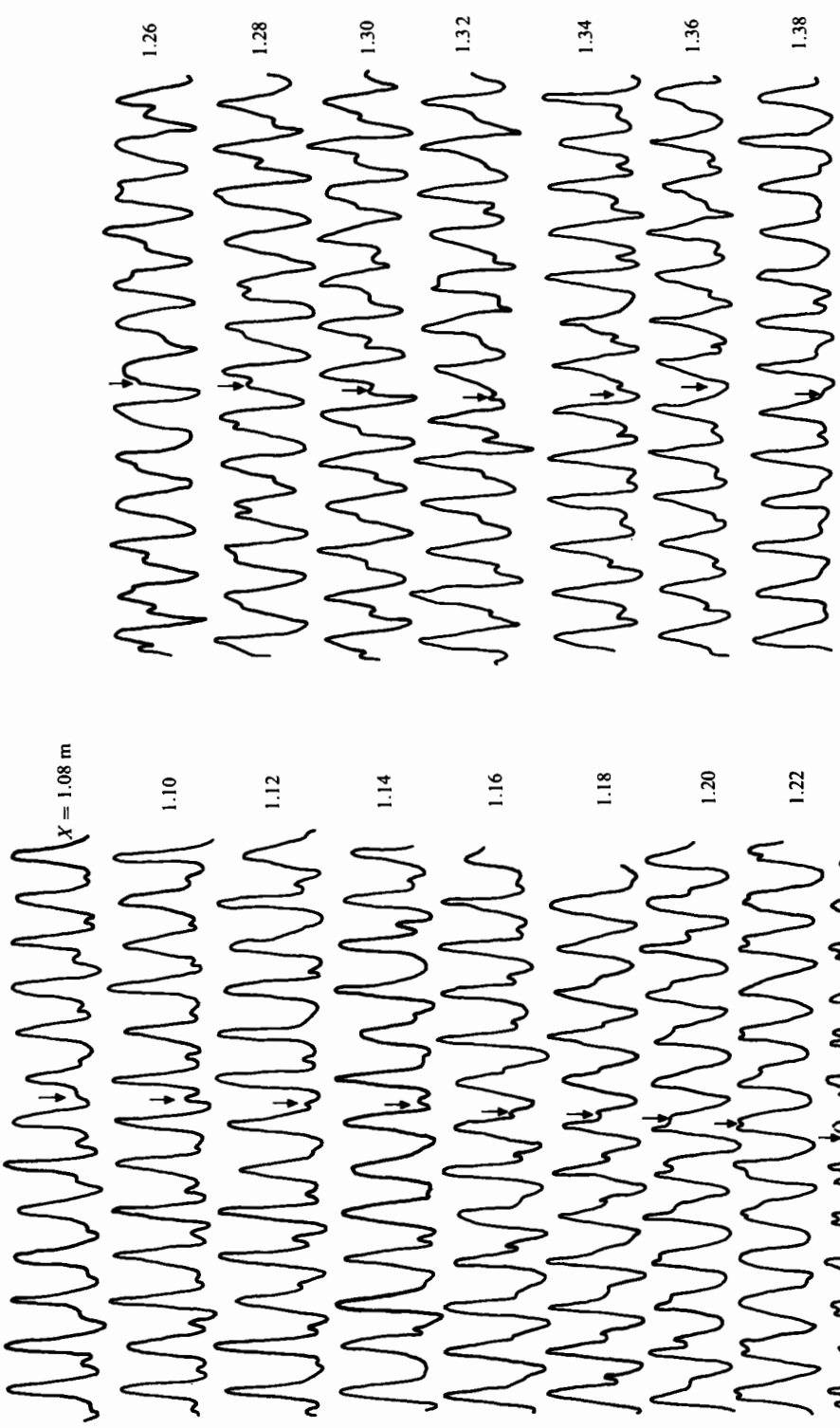

FIGURE 12. Typical waveforms for $W = 1.25$ m/s ($C/W = 0.73$) at different fetch values lying between $X = 1.08$ m and 1.38 m.

Finally it was found that the measured values C_D and C_R are close to the respective values $\frac{1}{2}(W+C_{th}) = \frac{1}{2}(1.25+0.78) = 1.02$ m/s and $\frac{1}{2}(W-C_{th}) = 0.24$ m/s predicted by the analytical models for the downstream and the upstream (or downstream) wave components.

This result strongly suggests that, when the resonance condition is not satisfied, the three wave components found analytically combine to produce two components propagating respectively at $\frac{1}{2}(W+C_{th})$ and $\frac{1}{2}(W-C_{th})$. Clearly, both celerities depend upon the wind velocity.

The experimental work we have done showed mainly that a water-surface wave may almost instantaneously be generated by an air-flow perturbation through resonant excitation. If the resonance condition is not satisfied, the water-surface oscillation appears to be the combination of a downstream wave and an upstream (or downstream) wave with propagation celerities depending upon the wind velocity. These non-resonant waves may possibly play an important role in the evolution of various wave fields, including the wind waves.

The authors would like to thank Dr A. Ramamonjiarisoa for supervising this work, Dr E. Mollo-Christensen, and particularly Professor O. M. Phillips, for their helpful comments on the manuscript, Dr Gelci for his various and useful remarks and all I.M.S.T. technical staff for their help and various contributions, J. Quaccia for the vortex-generator construction, M. Bourguel for his assistance in digital procedures and A. M. Rugiero for drawings and for typing the manuscript. This work was supported by the Etablissement d'Etudes et de Recherches Météorologiques and the Centre National de la Recherche Scientifique (France).

REFERENCES

Betchov, R. & Criminale, W. O. 1967 *Stability of Parallel Flows*. Academic.

Burg, J. P. 1968 A new analysis technique for time series data. Nato Advanced Study Institute on Signal Processing. Enschede, Netherlands.

Collis, J. C. & Williams, M. J. 1959 Two-dimensional convection from heated wires at low Reynolds numbers. *J. Fluid Mech.* **6**, 357–384.

Favre, A. & Coantic, M. 1974 Activities in, and preliminary results of, air–sea interactions research at I.M.S.T. *Adv. Geophys.* **18A**, 391–405.

Gelci, R., Ramamonjiarisoa, A. & Hervouet, J. Y. 1983 Generation de vagues de gravité par des allées de tourbillons aériens mobiles. To be published in *J. Mécanique Théorique et Appliquée.*

Giovanangeli, J. P. 1980 A non dimensional heat transfer law for a slanted hot film in water flow. *Disa Info. n° 25*, Copenhagen, Denmark.

Goldstein, S. (ed.) 1957 *Modern Developments in Fluid Dynamics*. Clarendon.

Hasselmann, K. 1968 Weak interaction theory of ocean waves. In *Basic Developments in Fluid Dynamics* (ed. H. Holt), p. 117. Academic.

Lacoss, R. T. 1977 Autoregressive and maximum likelihood spectral analysis methods. In *Aspects of Signal Processing* (ed. G. Tacconi), part 2, pp. 591–614. Holland: Dordrecht.

Longuet-Higgins, M. S. 1977 Some effects of finite steepness on the generation of wave by wind. In *A Voyage of Discovery: George Deacon 70th Anniversary Volume* (ed. M. Angel), pp. 393–403. Pergamon.

Memponteil, A. 1983 Réponse d'une surface d'eau à des mouvements tourbillonnaires dans l'écoulement d'air adjacent. Thèse de Doctorat de 3° Cycle, Université d'Aix-Marseille II.

Miles, J. W. 1960 On the generation of surface waves by turbulent shear flow. *J. Fluid Mech.* **7**, 185–204.

MOLLO-CHRISTENSEN, E. & RAMAMONJIARISOA, A. 1978 Modeling the presence of wave groups in a random wave field. *J. Geophys. Res.* **83**, 4117–4122.

PHILLIPS, O. M. 1957 On the generation of waves by turbulent wind. *J. Fluid Mech.* **2**, 417–445.

PHILLIPS, O. M. 1966 *Dynamics of the Upper Ocean.* Cambridge University Press.

SEDOV, L. 1973 *Mécanique des Milieux Continus.* M.I.R. Ed., Moscow.

STOKER, J. J. 1957 *Water Waves.* Interscience.

ULRYCH, T. J. & JENSEN, O. 1974 Cross spectral analysis using maximum entropy. *Geophys.* **39**, 000–000.

VAN DEN BOS, A. 1971 Alternative interpretation of maximum entropy spectral analysis. *IEEE Trans. Inform. Theory*, vol. I, t. 17.

WOOD, C. J. & KIRMANI, S. F. A. 1970 Visualization of heaving aerofoil wakes including the effect of a jet flap. *J. Fluid Mech.* **41**, 627–640.